Geophys. J. Int. (2007) **168,** 710–722 doi: 10.1111/j.1365-246X.2006.03212.x

Classification of seismic patterns in a hierarchical model of rupture: a new phase diagram for seismicity

Clément Narteau

Laboratoire de Dynamique des Systèmes Géologiques, Institut de Physique du Globe de Paris, 4, *Place Jussieu, Paris, Cedex* 05 75252, *France.*
E-mail: narteau@ipgp.jussieu.fr

Accepted 2006 September 4. Received 2006 September 4; in original form 2001 November 22

SUMMARY

I present a detailed description of the temporal properties of seismicity in a hierarchical model of rupture incorporating healing and faulting. At the microscopic scale, a stochastic process controls transitions between a solid and a broken state with respect to the local stress. From the distribution of broken elements, geometric rules of interaction determine the state of fracturing of domains of larger dimensions and the shape of the stress redistribution. Then, any point in space evolves with respect to its state of stress and its state of fracturing measured at different length scales. Applied to a single fault zone under a constant loading rate, this model of seismicity reproduces the main characteristics of the seismic catalogues: Gutenberg–Richter law for the magnitude–frequency relationship, Omori law for the aftershock decay rate, clustering of major events, swarms of earthquakes, seismicity of creeping segment and seismic noise. I infer that the control parameter is the dimensionless parameter A, the ratio between a characteristic time of healing and a characteristic time of loading. Following the magnitude of A, different seismic scenarios emerge: if $A \approx 1$, the system is in a critical state and largest events can occur over a wide range of timescales (e.g. clustering of major events); if $A < 1$, the system is in subcritical states controlled by faulting and seismic precursor are frequently observed; if $A > 1$, the system is in subcritical states controlled by healing and the fault zone may be creeping. One particular feature is that the amplitude of the stress stored in the fault zone decreases and the frequency of large events increases as the critical state is approached. This can be interpreted as a weakening process. I propose a new phase diagram of seismicity to illustrate an alternative to the classical seismic cycle picture.

Key words: aftershocks, earthquakes, faulting, fractals, seismicity.

1 INTRODUCTION

A striking feature of tectonic faulting is that different fault segments may accommodate displacement by different mechanisms which can be characterized by stick-slip seismic or creep behaviour. Creep is analogous to slow and permanent deformation, while stick-slip movement along seismic faults is highly discontinuous in time. Transient slip rate have been recorded along creeping fault segments, and, most of the time, it can be related to changes in seismicity (Murray & Segall 2005). In a vast majority of cases, earthquakes occur in clusters. In these clusters, the temporal distribution of events seems to be related to earthquake magnitude. Two widely known examples are the magnitude–frequency distribution (i.e. the Gutenberg–Richter law) and the aftershock decay rate (i.e. the Omori law). In both cases, there is no getting round power-law regimes which support the existence of long-range correlation in the seismogenic crust.

In the last decades, a large amount of work has been devoted to the analysis of the temporal distribution of earthquakes. Some studies follow a theoretical elastodynamic approach (Ben-Zion 2001) in which heterogeneities in structure, composition and friction cause different levels of complexity of seismicity. Others, view earthquake distribution as a result of a non-linear dynamic system (see references in Main 1996; Turcotte 1999) but rarely describe in detail the physical properties of a fault network. Nevertheless, they reproduce many aspects of the seismic catalogues (e.g. the Gutenberg–Richter law and/or the Omori law) within a stationary statistical state of self-organized criticality. In this paper, I present a classification of different seismic patterns in a cellular automaton with long-range interactions in which the hierarchy of faulting structures has been imposed. Following Allègre *et al.* (1982), the rupture is considered as a critical phenomenon and real-space renormalization techniques are applied.

A critical phenomenon is characterized by its critical point at a critical value of a control parameter. From below and above this critical value, the power law of the event-size distribution is truncated and the correlation length decreases. At the critical point, the system is self-similar, the event-size distribution follows a power law, the correlation length becomes infinite, and microscopic fluctuations

can result in major changes at all length scales. Such a sensibility is a insuperable obstacle to classical theories and their predictions fail in the immediate vicinity of the critical points. The basic idea of the renormalization group theory is to recalculate a limited number of physical quantities at increasingly larger length scales. Thus, it is possible to deal with problems involving lot of degrees of freedom and structures on a variety of length scales (Wilson 1983), especially close to a critical point. Overall, the renormalization group theory has been successfully applied in statistical physics to study thermally activated critical phenomena such as the ferromagnetic–paramagnetic transition (Kadanoff 1966), and in the percolation theory to study purely geometric connectivity phenomena (Reynolds *et al.* 1977).

Real-space renormalization techniques provide the simplest approach to the renormalization group theory. According to an integer $\mathcal{R}$, defined as the renormalization factor, the elementary lattice of spacing l is divided up into independent lattices of spacing $\mathcal{R}l$, $\mathcal{R}^2l$, $\mathcal{R}^3l$ and so on. Thus, a hierarchical system of embedded cells can be described from the smallest length scale $k = 0$ to the largest length scale $k = \mathcal{K}$. Within a $\mathcal{D}$-dimensional system, each cell of length scale k is a disjoint block of $\mathcal{R}^{\mathcal{D}k}$ cells of the microscopic length scale as well as a disjoint block of $\mathcal{R}^{\mathcal{D}(k-k')}$ cells of length scale k' (Fig. 1). Finally, cells of different dimensions are assigned a state, and a renormalization transformation determines the state of any cell from the configuration of the corresponding block of cells of the smaller dimension.

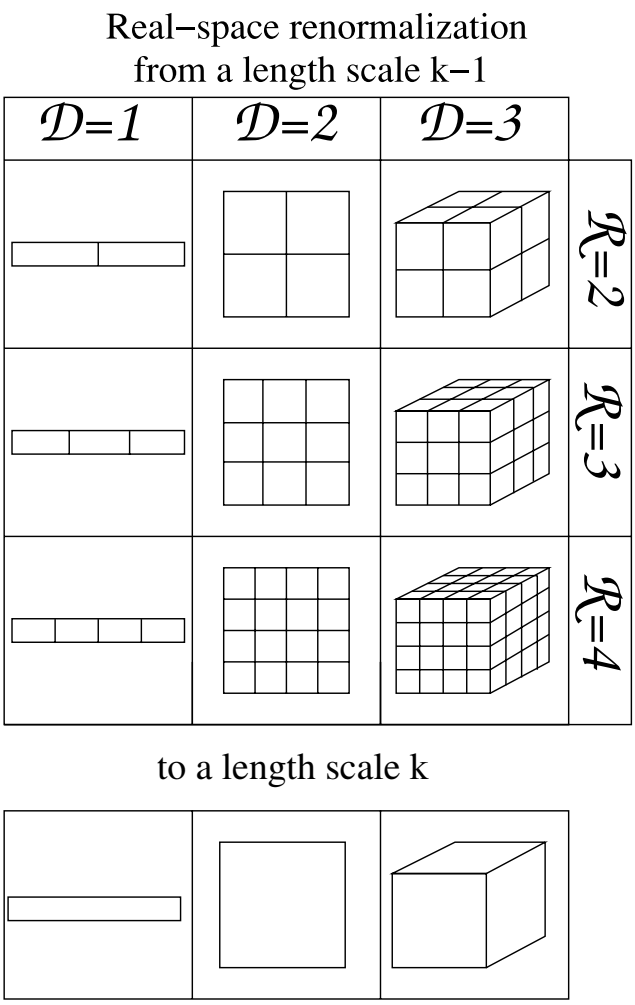

Figure 1. Real-space renormalization technique: each block of R^D cells of a smaller length scale $k - 1$ is linked to a single cell of length scale k.

With similar hierarchical systems as those used by Reynolds *et al.* (1977, 1978), Allègre *et al.* (1982) introduced the real-space renormalization method to the rupture problem. In their model, the control parameter is the density of broken cells at the microscopic length scale (i.e. microfractures). It evolves according to the applied stress field and determines the density of fractures at increasingly larger length scales via a polynomial expression P. In case of a percolation-type fracture criterion, P is a monotonic increasing function with a critical point at $P(x) = x$ (i.e. the density of fracture is the same at all length scales). If $P(x) > x$, the density of fracture increases with respect to the length scale. If $P(x) < x$, this density decreases. As a result, the macroscopic probability to be broken jumps from 0 to 1 when the density of broken cells exceeds a critical density at the microscopic length scale. Thus, close to this critical density, microscopic fluctuations (new microfractures) may produce macroscopic phenomena (earthquakes). Allègre *et al.* (1995) apply this concept to the modelling of an instability leading to an earthquake and Blanter & Shnirman (1997) describe different critical behaviours according to different failure criteria.

Later, hierarchical systems have been used to model structural properties of fault zones and the earthquake phenomenology (Narteau *et al.* 1997; Gabrielov *et al.* 2000; Turcotte *et al.* 2000). In these models, inspired by a fluid mechanics terminology (Kolmogorov 1941a,b; Kraichnan 1967), a cascade is the transfer of a physical parameter through a wide range of spatial scales. An inverse cascade corresponds to a transfer from smaller to larger length scales. A direct cascade corresponds to a transfer from larger to smaller length scales. For example, in Narteau *et al.* (2000)

(i) The continuous stress transfer induced by the tectonic loading and the stress perturbations induced by earthquakes contribute to the appearance of microfractures. This is described as a direct cascade of stress redistribution.

(ii) The fracturing phenomena depend on evolving configurations of microfractures and their geometric organization at different length scales. This implementation of a real-space renormalization technique is described as an inverse cascade of fracturing and healing.

Using a similar approach, this paper provides a detailed description of the temporal properties of the seismicity produced by a fault zone under constant loading. In this model, the seismic regime is governed by the magnitude of a control parameter and a critical point can be identified. Hence, it is possible to predict different types of earthquake sequences from below and above the critical point. More specifically, stick-slip seismic and creep behaviour can be discussed with respect to the magnitude of the loading process.

2 MODEL OF A FAULT ZONE

The displacements imposed at the boundary of a tectonic domain by the motion of plates generate compressive principal stresses σ_1, σ_2, σ_3 which are north–south, vertical and east–west, respectively. Pre-existing damages in one direction favour a single orientation for active faulting, and only dextral strike-slip faults with an inclination Θ from σ_1 can develop and accommodate the deformation along narrow zones (hereafter called fault zones). Such a localization process of the deformation is modelled by Narteau (2006).

Meanwhile, this paper focuses on the temporal properties of the seismicity observed in a model of a single fault zone. This model

of rupture including faulting and healing has previously been described in Narteau *et al.* (2000), where a more detailed description than the brief summary below is presented. Along the fault zone, it is assumed that fractures of different length scales appear in hierarchically organized cells. All these fractures have a specific orientation (i.e. the orientation of active faulting at the inclination Θ from σ_1) and a single type of rupture mechanism (dextral strike-slip) in order to study the temporal properties of the stress dissipation from a scalar stress field without perturbation.

2.1 The hierarchical system: a discrete representation of a fault zone

At the length scale $k = \mathcal{K}$ of the fault zone, the whole volume is modelled by a $\mathcal{D}$-dimensional cell ($\mathcal{D} = 2$). This cell is subdivided in $\mathcal{R}^{\mathcal{D}}$ cells of the same shape, $\mathcal{R}$ being the renormalization factor ($\mathcal{R} = 2$, see Fig. 1). For each cell of smaller dimension, the same operation is repeated until a hierarchical system of cells with $\mathcal{K}+1$ different length scales is obtained. At the smallest length scale $k = 0$, opposite tectonic motions on both sides of the fault zone can initiate microfractures with a characteristic length l_0. It follows that the characteristic dimension of a cell of the length scale k is $l_k = l_0\mathcal{R}^k$.

Since this hierarchical system is a simplified representation of 3-D brittle fault zone, it is not the intent to precisely locate or describe any cells. What matters are their relative positions or states of fracturing and how they interact at all length scales.

2.2 The elementary scale: an evolving population of microfractures

At the smallest length scale of the hierarchical system (hereafter called the elementary scale) a cell is characterized by a state and a local accumulated shear stress $\sigma(t)$. The solid state corresponds to an unfractured or consolidated medium. The broken state corresponds to a microfracture. According to the magnitude of the tectonic motions on both sides of the fault zone, the local accumulated shear stress increases at a constant rate $\dot{\sigma}$:

$$\sigma(t + \Delta t) = \sigma(t) + \dot{\sigma}\,\Delta t.$$

The local shear stress accumulated by a broken cell cannot exceed a friction threshold σ_b, and, if $\sigma(t) = \sigma_b$, the excess of stress is continuously released by aseismic slip (creep). Then the evolution of the system is determined by local transition rates between the two possible states (see Table 1):

(i) The *solid* $\longrightarrow$ *broken* transition (fracturing). Above a fracturing threshold σ_s the accumulated shear stress produces motion along a microfracture (the rupture). A local microscopic stress drop $\Delta\sigma$ is associated with this motion.

Table 1. All the possible transition rates associated with the *solid* $\longrightarrow$ *broken* and the *broken* $\longrightarrow$ *solid* transitions. $\sigma(t)$ and σ_s are the local shear stress and the fracturing threshold, respectively. β is the healing rate and has the dimension of frequency. k_s is a constant with also a dimension of frequency and δ_s is a phenomenological material constant (Narteau *et al.* 2002).

	$\sigma(t) < \sigma_s$	$\sigma(t) > \sigma_s$
Solid	0	$k_s\left[\dfrac{\sigma(t)-\sigma_s}{\sigma_s}\right]^{\delta_s}$
Broken	β	β

(ii) The *broken* $\longrightarrow$ *solid* transition (healing). Compaction in presence of fluids, grain growth or crack crystallization are some of the microscopic physical–chemical processes at the origin of healing. It induces a strengthening of pre-existing fractures at all length scales through geometrical blocking. This healing process is considered uniform and constant with a typical $1/\beta$ characteristic timescale.

2.3 The inverse cascade of fracturing or strengthening

Cells at all length scales of the hierarchical system are solid or broken. The solid state corresponds to an unfractured or consolidated medium, the broken state corresponds to a fracture that forms from the merging of smaller ones. Hence, a cell of a larger length scale is broken if the corresponding block of cells of the smaller length scale is in a critical configuration (Fig. 2b). Thus, from the configuration of broken cell at the elementary scale, it is possible to determine the state of all cells at increasingly larger length scales.

Practically, when a cell of the elementary scale operates a transition, the whole configuration of the hierarchical system is recalculated from the smallest to the largest length scale by checking all the configurations of broken cells. At the largest length scale at

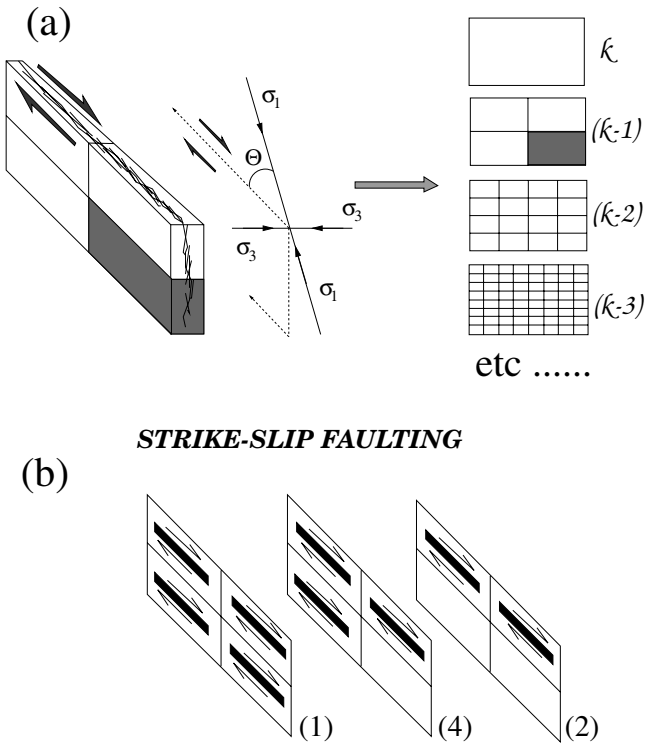

Figure 2. (a) A model of a fault zone: fractures of different length scales appear in hierarchically organized cells. Each cell of a length scale $(k+1)$ is linked to a group of cells of the smaller length scale k (see Fig. 1 with $R = 2$ and $D = 2$). In such a hierarchical system, all fractures are oriented at the inclination Θ to the maximum compressive stress σ_1 which is north–south. (b) Configurations of broken cells associated with a broken state at the larger length scale. The number in brackets corresponds to the number of critical configurations with the same number of *broken* cells. Following Allègre *et al.* (1982), the polynomial expression is $P(x) = 1 - (1 - x^2)^2$ and the critical density of microfractures is approximately equal to 0.62.

which a cell experience a transition, this transition is defined as an earthquake or a fracture healing:

(i) *Earthquake*: following the perturbation associated with the *solid* $\longrightarrow$ *broken* transition at the elementary scale, the organization of pre-existing fractures allows for an earthquake with a dimension l_e of the largest length scale k_e at which a *solid* $\longrightarrow$ *broken* transition has taken place. The location of the hypocentre is given by the position and the time of the transition of the elementary scale which triggered the event. The magnitude is proportional to k_e because the slip and the rupture area are taken proportional to l_e and l_e^2, respectively.

(ii) *Healing of a fractured rock mass*: following a *broken* $\longrightarrow$ *solid* transition at the elementary scale, the new organization of microfractures results in a geometrical blocking of a fractured rock mass which has a dimension l_e of the highest scale k_e where a *broken* $\longrightarrow$ *solid* transition has taken place. The new solid cells recover their strength and their fracturing potential.

Critical configurations are associated with a percolation rule defined with respect to the orientation of the rupture (Fig. 2b). Theoretically, and for an infinite number of cells, such a failure criterion has the same properties as the failure criterion adopted by Allègre *et al.* (1982). At the critical density of microfractures (i.e. the ratio between the number of broken cells and the total number of cells), the density of fractures at all length scales is the same (self-similarity). Under the critical density of microfractures, the density of fractures decreases with increasing length scale. Above the critical density of microfractures, the density of fractures increases with increasing length scale. Around the critical density of microfractures, infinitesimal variations of the density of microfractures can produce earthquakes of the largest length scale.

Nevertheless, for an evolving population of broken elements at the microscopic length scale, more than the density, the exact configuration of the broken elements is preponderant. Indeed, for the same number of broken elements (i.e. density of microfractures), many different states may be observed at larger length scales. For example, far from the critical density, rare events may occur and affect the seismic patterns over long time, while, close to the critical density, repetition and absence of large earthquakes may be observed. Meanwhile, the state of stress and the state of fracturing evolve from each other by many ways, and major events may occur on different configurations of stress.

2.4 The direct cascade of stress redistribution

After an earthquake, redistribution of stress takes place in the neighbourhood of the active fracture within a zone proportional to the dimension of the event. From the scale of this earthquake to the elementary scale, a stress redistribution pattern is applied to any cell which operates a *solid* $\longrightarrow$ *broken* transition. The stress redistribution pattern is obtained by scaling of a mask which is defined by the strike of the rupture and which could be characterized by an increase of the shear stress along the strike of the rupture and a decrease in the perpendicular direction. The scaling is done with respect to a scaling exponent related to the renormalization factor. The mask consists on four parameters in order to take into account the anisotropic stress redistribution on nearest and next nearest neighbours. The magnitudes of these parameters are determined from theoretical stress near idealized fractures in uniform rocks.

Irrespective of the configuration of solid and broken cells and the size of the event, this redistribution always creates heterogeneities of the stress field at every length scale. Such an heterogeneous stress field is responsible for the shape of the aftershock decay rate over short and long times (Narteau *et al.* 2002, 2003, 2005).

Table 2. Model parameters values.

R	2
D	2
σ_b	100 bars
σ_s	110 bars
k_s	10^{-4} s^{-1}
δ_s	3

2.5 The dynamic system

At each iteration, only one cell of the elementary scale makes a transition from one state to the other. Hence, two random numbers determine the time step, and the location of the cell of the smallest length scale which undergoes this transition. More precisely, if $\alpha^i(t)$ is the transition rate of the ith elementary cell at time t (Table 1):

(i) The event rate (i.e. $1/\Delta t$) is proportional to

$$\sum_{j=1}^{\mathcal{R}^{\mathcal{DK}}} \alpha^j(t),$$

(ii) The probability for the ith cell to make the transition is

$$\frac{\alpha^i(t)}{\sum_{j=1}^{\mathcal{R}^{\mathcal{DK}}} \alpha^j(t)},$$

where $\mathcal{R}^{\mathcal{DK}}$ is the number of elementary cells.

The stochastic approach renders the complexity and the multitude of physical processes involved in the fracturing of brittle rocks at the microscopic scale. Interestingly, the random component allows of low-probability events to occur occasionally.

At time $t = 0$, the system is in a homogeneous state. All elements are intact and stresses, fracturing thresholds and friction thresholds are uniform (see Tables 1 and 2). The first cell to fail is chosen at random. Later, the failure rate evolves according to the distribution of stress, and, the healing rate evolves according to the number of broken elements. Thus, during transient phases small time steps may capture all details, and, for a large number of elementary cells, $\mathcal{R}^{\mathcal{DK}} \to \infty$, a continuous-time method is approached.

3 PROPERTIES OF SEISMICITY ALONG A FAULT ZONE UNDER CONSTANT LOADING RATE

In this section, different properties of the seismicity of the model are described according to the magnitude of a single free parameter A. This dimensionless parameter is defined as the ratio of the external loading rate and the product of the healing rate and the constant local stress drop:

$$A = \frac{\dot{\sigma}}{\beta \Delta\sigma}. \tag{1}$$

$\Delta\sigma/\dot{\sigma}$ is the characteristic timescale to recover the microscopic local stress drop with the uniform external loading rate and, as said above, $1/\beta$ is the characteristic timescale of microscopic healing. Thus, A is a measure of the ratio between the characteristic timescale of

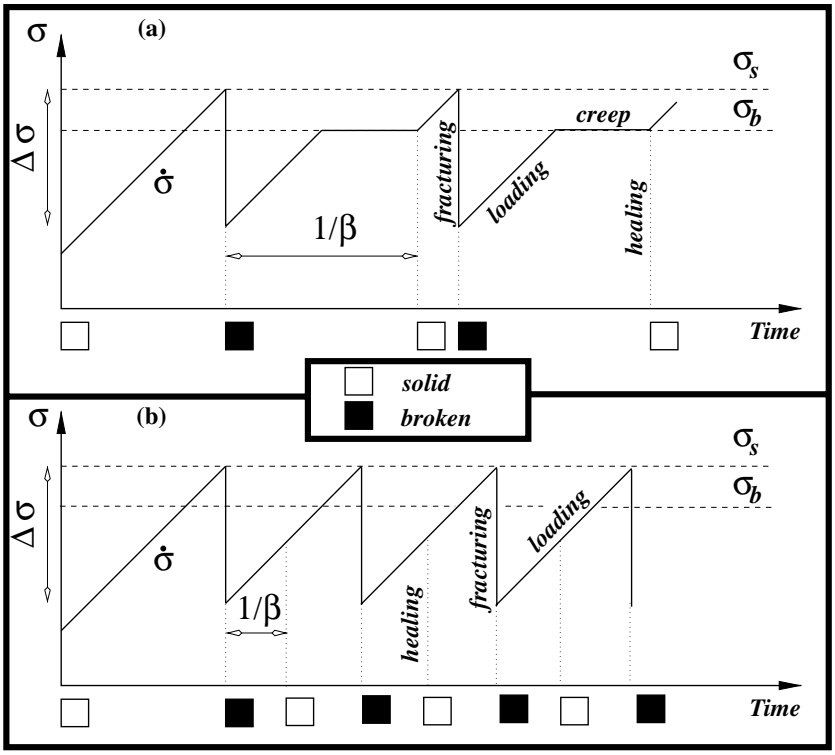

Figure 3. Evolution of the stress and of the state of fracturing of a single cell of the smallest length scale for (a) $1/\beta > (\Delta\sigma - (\sigma_s - \sigma_b))/\dot{\sigma}$ and (b) $1/\beta < (\Delta\sigma - (\sigma_s - \sigma_b))/\dot{\sigma}$. $\dot{\sigma}$ is the external loading rate, β is the healing rate, $\Delta\sigma$ is the local stress drop, σ_s is the fracturing threshold and σ_b the friction threshold. This schematic diagram illustrates the local constitutive rules of the model without the stochastic component.

healing and the characteristic timescale of loading. It indicates the state of fracturing of an elementary cell after it has recovered the stress drop through the loading process (broken if $A > 1$, solid if $A < 1$).

Like the Reynolds number in fluid mechanics, the basic properties of the model are determines by the A-value. In contrast to the Navier–Stokes equation, in which the status of the Reynolds number is demonstrated from the structure of the equation, the parameter A can only be inferred from the rules of the model or via systematic numerical experiments. In particular, the evolution of a single cell without the stochastic component may help in understanding the importance of the parameter A (Fig. 3). Interestingly, this evolution only illustrates the small-scale dynamics and the local constitutive rules of the model without considering the cascade mechanisms and the random fluctuations. Fig. 3(a) shows that if $1/\beta > [\Delta\sigma - (\sigma_s - \sigma_b)]/\dot{\sigma}$, the next failure is delayed and creep occurs. If not the recurrence time is simply $\Delta\sigma/\dot{\sigma}$ (Fig. 3b) as in the linear time-dependent earthquake prediction model of Shimazaki & Nakata (1980). Therefore, the state of an elementary cell after it has recovered an amount of stress equal to $\Delta\sigma - (\sigma_s - \sigma_b)$ is key. In order to reduce the number of variables, the magnitudes of σ_s and σ_b are chosen close to each other such that $\Delta\sigma - (\sigma_s - \sigma_b) \approx \Delta\sigma$. Then, A, the ratio between $1/\beta$, the characteristic time of healing, and $\Delta\sigma/\dot{\sigma}$, the characteristic time of loading, becomes crucial.

In the numerical experiments presented below, A covers seven orders of magnitude while $\dot{\sigma}$ and β vary by more than nine and three orders of magnitude, respectively. Values of $\Delta\sigma$ range from 10 to 40 per cent of the fracturing threshold.

Figs 4 and 5 show the evolution of three parameters versus A. These parameters are calculated over a long time period T [$T \gg \max(\Delta\sigma/\dot{\sigma}, 1/\beta)$] and from a large number of seismic cycles. These three parameters are

(i) The average density of microfractures,

$$D = \frac{1}{T}\int_0^T d(t)\,dt, \tag{2}$$

where $d(t)$ is the density of broken cells at the elementary scale at time t (Fig. 4a).

(ii) The average shear stress normalized by the fracturing threshold,

$$S = \frac{1}{T}\int_0^T s(t)\,dt, \tag{3}$$

with,

$$s(t) = \frac{\sum_i^{\mathcal{R}^{\mathcal{DK}}} \sigma_i(t)}{\sigma_s \mathcal{R}^{\mathcal{DK}}},$$

where $\sigma_i(t)$ is the shear stress of cell i of the elementary scale at time t and $\mathcal{R}^{\mathcal{DK}}$ is the number of cells at the elementary scale of the hierarchical system (Fig. 4b).

(iii) The break of slope of the magnitude–frequency relationship,

$$B = b_l - b_s, \tag{4}$$

where b_l is the b-value (i.e. the slope of the magnitude–frequency relationship) of earthquakes with a magnitude larger than M_c, and b_s is the b-value of earthquakes with a magnitude smaller than or equal to M_c (Rotwain *et al.* 1997). M_c is set as 4 to obtain two populations of earthquakes over a equivalent interval of magnitude (Fig. 5). If $B = 0$, the magnitude–frequency relationship is linear and the

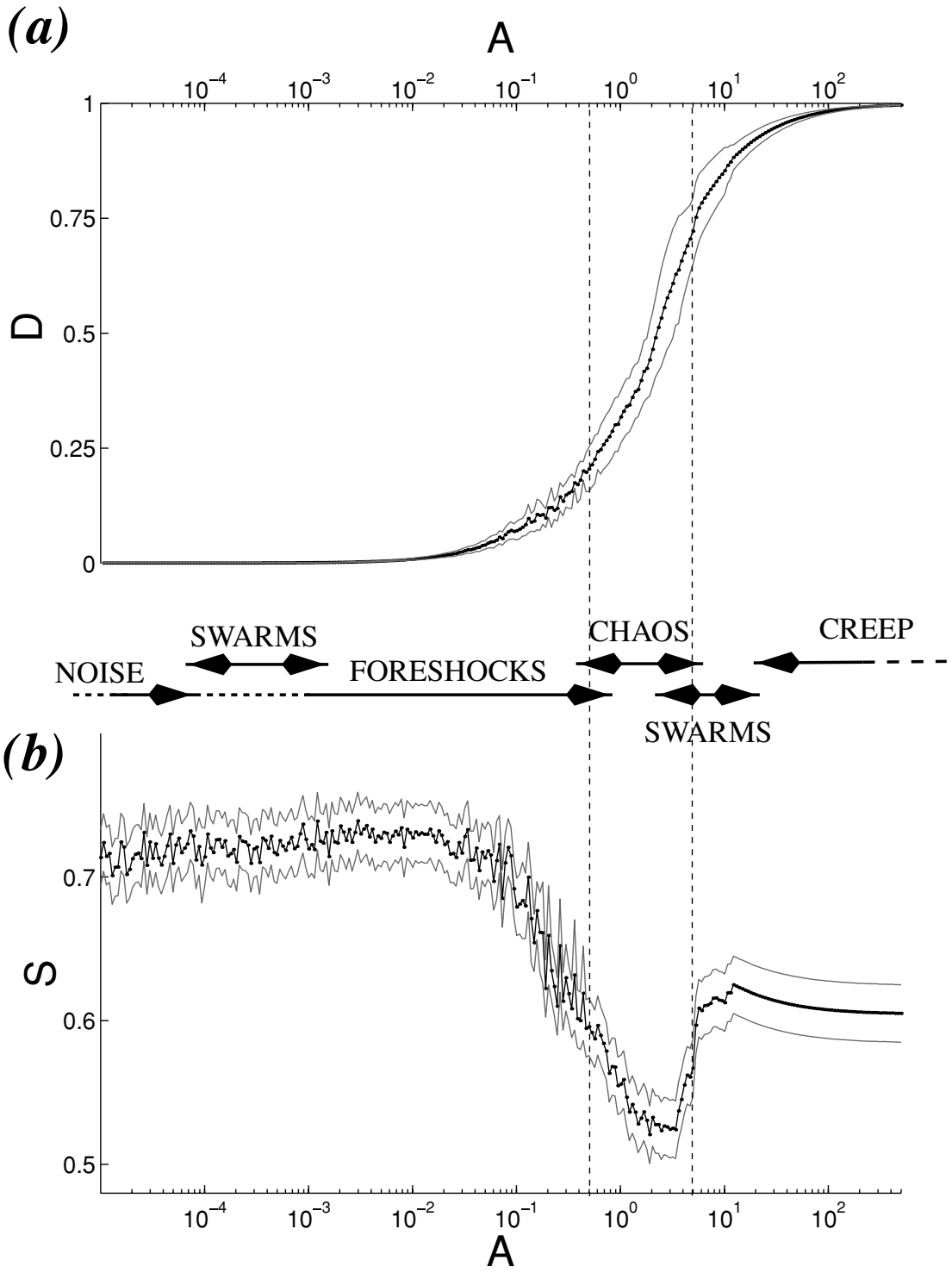

Figure 4. (a) Evolution of the average density of microfractures D (eq. 2) and (b) evolution of the average shear stress S (eq. 3) versus A, the ratio between the loading rate and the healing rate (eq. 1). Between these figures, a legend indicates different classes of seismic behaviours corresponding to different ranges of A. For each of the 200 values of A a dozen realizations has been performed exploring different values of ($\dot{\sigma}$, β, $\Delta\sigma$) (see text). The dotted black lines are the mean value while the grey lines limit the standard deviation envelops. The dashed lines limit the critical states at $A = 0.5$ and 5.

system is at a critical point. If $B < 0$ the magnitude–frequency relationship is truncated, the correlation length is finite and the system is in a subcritical state characterized by a deficit of large earthquakes.

For different values of A, representative earthquake sequences are shown in Fig. 6. In addition, the phase diagram in Fig. 7(a) illustrates how the density of microfractures and the total amount of elastic energy stored in the system evolved from one another. On

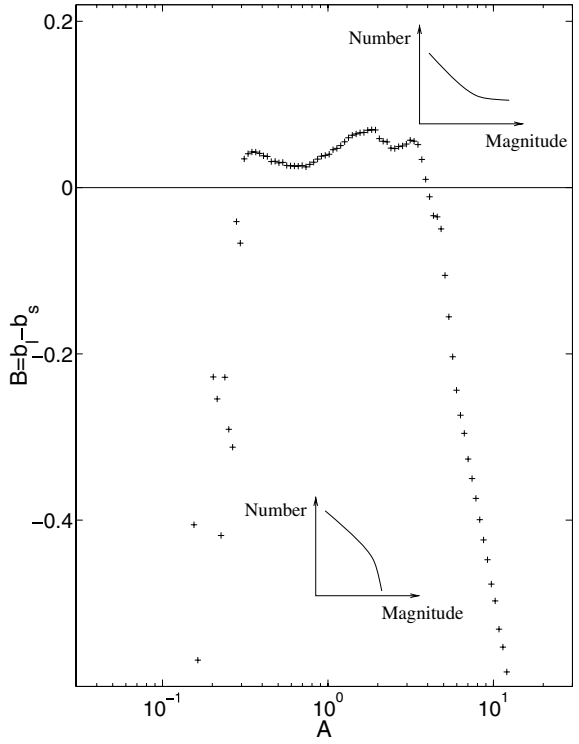

Figure 5. Evolution of the break of slope of the magnitude–frequency relationship B versus A, the ratio between the loading rate and the healing rate. The B-value is equal to the difference between b_l and b_s, the b-values for earthquakes with a magnitude larger and lower than M_c. The top and bottom insets show typical distributions for which this difference is, respectively, positive and negative.

this phase diagram the axes are the density of microfractures and the total shear stress stored within the fault zone. The trajectories describe the evolution of $[d(t), s(t)]$ for different values of A. In the phase diagram the centre of the concentric circles corresponds to the critical density of microfractures (Allègre *et al.* 1982) and to an averaged stress close to the fracturing threshold. The closer the trajectory is to the critical point, the larger is the magnitude of the earthquake. Numerical phase diagrams are also shown to validate the schematic ones (Fig. 7b).

In this model of a single fault zone, it is possible to identify different seismic regimes associated with stationary statistical states defined by $[D(A), S(A), B(A)]$. These classes of seismicity and their geophysical implications are discussed in the next sections for an increasing A-value.

3.1 Seismic noise, $A \ll 10^{-3}$

D is close to zero and S is relatively low. With increasing values of A, D and S slowly increase (Fig. 4). Only microseismicity is observed (Fig. 6a). Stress dissipation in small events is in equilibrium with the tectonic loading. The total amount of shear stress accumulated in the system is almost constant. In the phase diagram, the trajectory is dense and fuzzy (*point* trajectory of Fig. 7a) around a low value of $d(t)$ and a value of $s(t)$ which increases following A.

3.2 Seismic swarms, $A \sim 10^{-3}$

D is low, S has now a larger value (Fig. 4), and they continue to increase. Seismicity is dominated by swarms of earthquakes (Fig. 6b). In these clusters, the seismicity rate increases and decreases before and after few earthquakes of moderate magnitude. Each of them has its own aftershock sequence. Seismic swarms maintain high total shear stress but with significant fluctuations due to strong variations in the density of microfractures. This behaviour corresponds to the large and flat trajectory (*rectangular* trajectory of Fig. 7a). The swarm of seismicity is associated with a rapid increase in the density of microfractures without large stress drops. Then the stress recovers slowly, and the healing process is more active (remember that $A \ll 1$). Later, the stress increases, but, when the density of microfractures start to increase, a sufficient amount of stress is released to impede the fracturing process to reach the largest length scales of the system.

3.3 Large earthquakes with foreshocks, $10^{-3} \leq A \leq 0.5$

D continues to increase and S reaches a maximum value before it constantly decreases (Fig. 4). Large earthquakes occur and, in a vast majority of cases, they are preceded by foreshock and an acceleration of the seismic energy release (Fig. 6c). After these large earthquakes, an aftershock sequence is observed over long time. In the phase diagram, a *u-shaped* trajectory is associated with these large earthquakes with foreshocks and aftershocks (Figs 7a and b_1).

Let us start the description of this trajectory at the point closest to the centre of the phase diagram. The largest events occur when both the density of microfractures and the total shear stress reach their threshold values (darkest regions of the phase diagram). These events involve large stress drops (the main shock part of the trajectory). Aftershocks are associated with an increase in the density of microfractures and lower stress drops. The healing rate is higher than the loading rate (i.e. $A < 1$) and most of the loading occurs when the density of microfractures is low. A large amount of shear stress is finally stored in a low fractured fault zone. To eliminate the excess of shear stress in the fault zone, the rate of seismicity increases and most of the energy is dissipated by earthquake. Such an increase of the seismic rate corresponds, via an increase of the density of microfractures, to an organization of the fracturing at all length scales. This brings the system to the centre of the phase diagram (see the beginning of the paragraph).

Seismic swarms and large earthquakes with foreshocks and aftershocks are two types of sequences that differ only *a posteriori* by the magnitude of the largest earthquakes in the sequence. In fact, the location of earthquakes and the pre-existing stress heterogeneities control the shape of the acceleration of the seismic release. Then, for the same value of $A < 0.5$, different types of seismicity may be observed because of the intensity of the non-linear instabilities. For example, swarms and large earthquakes with foreshocks (Figs 6b and c) may both be present within the same domain at different time periods. As a consequence, it is difficult to identify an exact threshold of A between the occurrence of swarms and the occurrence of major earthquakes with foreshocks. This holds also for seismic noise. Nevertheless, in the seismic noise case, these instabilities from the reference state occur over a time period longer than 10^8 yr. They are neglected because, over such a long time, it is difficult to imagine a constant tectonic forcing.

When seismic swarms and large earthquakes preceded by an acceleration of the seismic release dominate, the B-value is negative but approaches zero with increasing A-value (Fig. 5). This negative B-value indicates a break of slope to steeper values at large

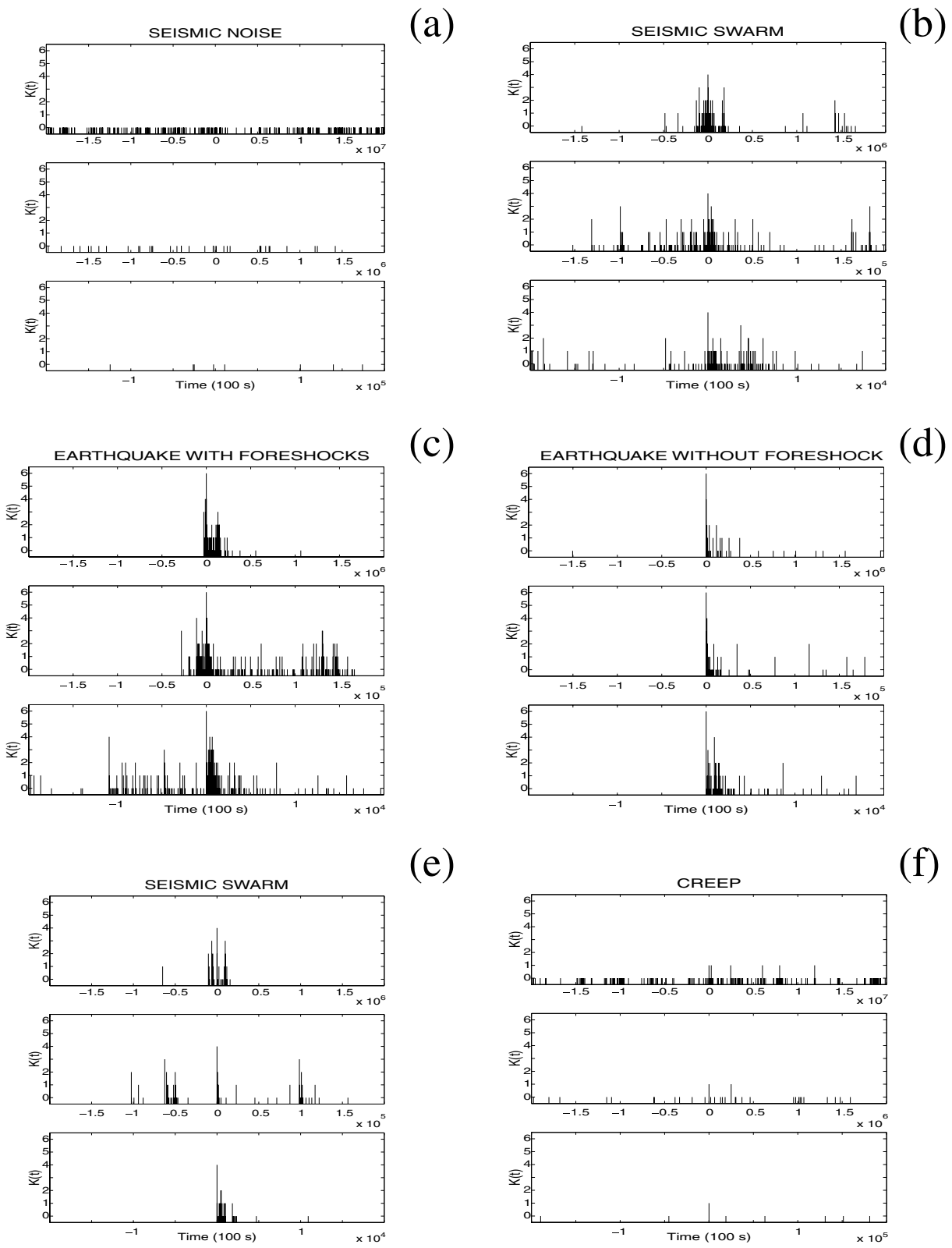

Figure 6. Characteristic seismic sequences of different classes of seismicity associated with different ranges of A. For each example, each bottom figure is a one order of magnitude zoom on the centre of the time window of the top figure. For an increasing A-value, the subfigures show: (a) seismic noise ($A < 10^{-3}$); (b) swarm of earthquake ($A \sim 10^{-3}$); (c) major earthquake with foreshocks ($10^{-3} \leq A \leq 0.5$); (d) major earthquake without foreshock ($0.5 \leq A \leq 5$); (e) seismic swarm ($5 \leq A \leq 10$) and (f) creep ($A \geq 10$). Note, for any large event ($K(t) > 3$), the quasi-systematic presence of its own aftershocks sequence.

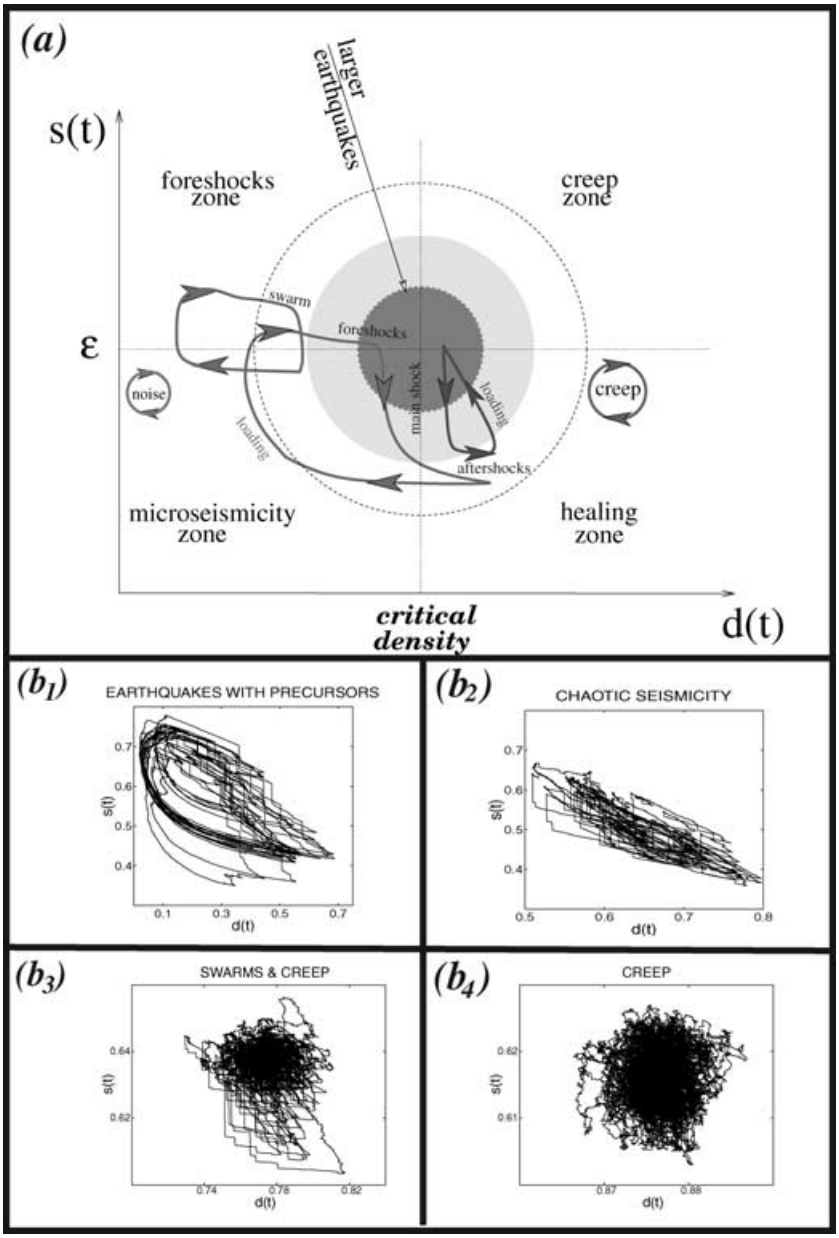

Figure 7. (a) schematic ($d(t)$, $s(t)$) phase diagram of seismicity along a fault segment. Different trajectories are associated with different A-values (i.e. different classes of seismicity see Figs 4 and 6). From the left to the right, the trajectories may include typical seismic sequences presented in Fig. 6(a) (noise, $A < 10^{-3}$), Fig. 6(b) (swarms, $A \sim 10^{-3}$), Fig. 6(c) (earthquakes with precursors, $10^{-3} \leq A \leq 0.5$), Fig. 6(d) (chaotic seismicity, $0.5 \leq A \leq 5$) and Fig. 6(f) (creep, $A \geq 10$). $\epsilon\,\sigma_s$ is the average shear stress stored in the system when largest events occur. Smaller concentric circles are associated with zones in which larger magnitude earthquakes occur (*critical point*). Following the stress and the density of microfractures, the phase diagram is divided in four zones; they are named from the phenomena observed along the trajectories passing through these zones. ($b_{\{1,2,3,4\}}$), real phase diagrams on limited time periods for typical seismic sequences presented in Fig. 6: (b_1), major earthquakes with precursors, $A = 0.3$ (Fig. 6c); (b_2), chaotic seismicity, $A = 3$ (Fig. 6d); (b_3), swarms and creep, $A = 6$ (Fig. 6e); (b_4), creep, $A = 20$ (Fig. 6f).

magnitude, a lack of large earthquakes and a finite correlation length within the system. Simultaneously, the b-value and the number of large events increase. These observations reveal a convergence towards self-similarity for an increasing A-value.

Finally, for any seismic cycle, if $A < 0.5$, the critical configurations are approached from below according to the density of microfractures. The system is in a subcritical state controlled by faulting. Then, to overcome rapid strengthening, failure is required to reach a critical configuration.

3.4 Chaotic seismicity, $0.5 \leq A \leq 5$

A sudden acceleration in the increase of D coincides with a minimum of S (Fig. 4). Seismicity is chaotic. Earthquakes of all magnitudes occur without typical foreshock patterns (Fig. 6d). Aftershocks and repetition of earthquakes are observed. The recurrence time between two major earthquakes varies over a wide range of timescales.

On the phase diagram, $d(t)$ and $s(t)$ are always near their threshold values in spite of intense fluctuations. A *triangle* trajectory is

clear (Figs 7a and b_2). The description of this trajectory starts at the point closest to the centre of the phase diagram. Main shocks and aftershocks display the same trajectory as those for lower values of A (see Section 3.3). However, the loading and the healing are now of the same order of magnitude. At the same rate, stress is accumulated and fractures are locked. Most of the loading occurs when the density of microfractures is high and, in the phase diagram, a straight trajectory is observed between majors events. The trajectory is always close to the critical point (i.e. self-organized criticality) and major events can repeat themselves quickly (i.e. seismic clustering). After these clusters, long time periods without major events can also be observed.

This behaviour occurs if $A \approx 1$ because the time period to compensate for the local stress drop by the external loading is of the order of magnitude of the physical–chemical healing time. This explains the minimum value of S. Because large earthquake can occur at lower stress a weakening process is at play.

For a chaotic seismicity, the break of slope of the magnitude–frequency relationship changes sign and the B-value is positive (Fig. 5). It shows that the seismicity is controlled by the occurrence of the largest earthquakes. As the frequency of large events reaches a maximum, there is a clear transition from a Gutenberg–Richter distribution to a 'characteristic' earthquake distribution with variable rather than constant recurrence time (Schwartz & Coppersmith 1984). At $B = 0$, such transitions are characterized by critical points. Thus, with respect to the B-value, there are two critical points, one for $A < 1$ and one for $A > 1$.

Most of the time, for $0.5 \leq A \leq 1$, the critical configuration is approached from below according to the critical density of microfractures. For $1 \leq A \leq 5$ the critical configuration is approached from above. Hence, from a subcritical state controlled by faulting ($A < 1$), the system operates a transition towards a subcritical state controlled by healing ($A > 1$). Then, more than failure, strengthening is required to reach a critical configuration.

3.5 Seismic swarms, $5 \leq A \leq 10$

D decelerates while S has recovered a higher value (Fig. 4). The system is highly fractured and seismicity is characterized by clusters of earthquakes. High magnitude earthquakes do not occur and most of the excess of stress is eliminated by friction.

These seismic swarms at a high density of microfractures are less dense than the seismic swarms at a low density of microfractures (Fig. 6e). The major difference with the seismic swarm at low density of microfractures is that this seismicity is essentially controlled by the healing and that, consequently, no regular recurrence times are observed.

The trajectory on the phase diagram is a mix between the *triangle* trajectory discussed above (Section 3.4) and a *point* trajectory corresponding to the creeping behaviour described below (Fig. $7b_3$).

The B-value is negative and continuously decreases with respect to A (Fig. 5). The critical configuration is never reached, but approached from above according to the density of microfractures. For higher value of A the absence of large events prevents accurate calculation of the B-value.

3.6 Creep, $A \geq 10$

D is closed to 1 while S converges to a constant value (Fig. 4). The fault zone is completely fractured and a continuous stress release is observed (creep). The seismicity in this creeping state is very low and only characterized by small earthquakes (Fig. 6f). In the phase diagram, this seismic pattern is a point trajectory at a high density of microfractures and a stress value defined by the friction threshold (Figs 7a and b_4).

4 DISCUSSION

This model couples essential ingredients of earthquake physics with coarse-grained physically based rules of interaction. It can easily points out realistic earthquake sequences and statistical behaviours of the seismicity from a limited number of parameters without requiring pre-existing small-scale heterogeneities. The implication for the Earth is that, despite complexities in rheology and composition, a large range of observational constraints on seismicity can results only from pattern of interactions between a population of fractures overtime.

Overall, the present study has demonstrated the crucial role of the parameter A in determining the nature and the predictability of seismicity. This control parameter arises from the local constitutive rules (Fig. 3), and it is defined as the ratio between the characteristic time of healing and the characteristic time of loading. If $A \approx 1$, the system is in a critical state and the critical configurations can be approached either from below or from above with respect to the microfractures density. No seismic precursors are observed but aftershocks are. If $A < 1$, the system is in a subcritical state and critical configurations are approached from below via failure. Seismic precursors may be observed. If $A > 1$, the system is in a subcritical state and critical configurations are approached from above via strengthening. Seismic precursors become rare and the stress is essentially eliminated by creep. Thus, from low to high A-value, the system is only in a critical state over a short range of magnitude of A and the critical configurations are increasingly approached from above. In real data, such observations support the idea that under given conditions the recurrence time of an earthquake may be constrained to a greater extent by healing rather than loading.

4.1 Analogies with the state of stress

Figs 4 and 5 show that with an increasing frequency of large events, the stress stored within the fault zone decreases. In other words, this means that stable zones have a high level of stress close to the fracturing threshold, while active fault zones have a low level of stress below the friction threshold. Because, these different zones coexist within plate boundary, intense variation of the stress would be expected.

Although this model is quasi-static, its results are consistent with the observation that faults with long-repeat times radiate more energy per unit fault length than those with short repeat times (Kanamori & Allen 1986; Scholz *et al.* 1986). In fact, if β and $\Delta\sigma$ are constant, large earthquakes occur at a lower stress level under a larger stress accumulation rate. Furthermore, at constant β-value or $\Delta\sigma$-value, major earthquakes with higher stress drops or healing rates occur within fault zones which have accumulated more stress. This dependence between healing and stress drop has been suggested by Scholz (1990). Another alternative which is related with the smoothing of the fault with displacement is discussed in Narteau (2006) from a model of formation and evolution of a population of faults.

From another point of view, the amount of shear stress stored in the system can be considered as a measure of the strength of the fault zone. In this case and for $A < 5$, it has been shown that larger loading rates increase the density of microfractures and drop the

strength of the fault segment to a lower level. This minimization can be described as a weakening process. Because of this higher density of microfractures large events occur more frequently. Therefore, an increase of the seismic activity is associated with a weakening of the zone of mechanical failure. A generalization of this process within a population of growing faults is suggested in Narteau (2006).

4.2 Synthetic catalogues

For a given fault zone, all the model parameters can be quantified from geophysical observations. In order to constrain the A-value, the external loading rate can be determined from large scale deformation and geodetic measurements, the healing rate can be fixed from the variation of the seismic velocity in the fault zone with time (Li *et al.* 1998) or from characteristic times of chemical reactions, the microscopic local stress drop can be inferred from laboratory experiments or seismology.

On the other hand, a wide range of seismic phenomena observed in real catalogues have been described: seismic noise, swarm of earthquakes, acceleration of seismic energy release, main shock with or without foreshocks, creeping fault segments. As shown in Narteau *et al.* (2000), this model also reproduces fundamental features of seismic catalogues: the Gutenberg–Richter law, the power-law aftershock decay rate Narteau *et al.* (2002, 2005), spatial-temporal clustering and the seismic cycle. Hence, the comparison between synthetic and real catalogues may provide the basis for a probabilistic prediction technique.

Nevertheless, the results of this paper are difficult to apply to real fault zones and historical seismic sequences. For example, high slip rate faults (i.e. high $\dot{\sigma}$ and $A > 5$) do not always exhibit creep, the variation of the b-value can lead to opposite conclusions (Smith 1986; Trifu & Mircea 1991) and a robust observation of acceleration of the seismic energy release along a single fault is yet to be made (see Section 4.3). Furthermore, it is difficult to compare the basic picture of a fault zone suggested in this paper (Fig. 2a) with geological observations at a length scale larger than 10 km. In fact, at this length scale, stress perturbations and fault interactions have to be taken into account in order to confront any numerical model with natural data. This is why, instead of working on some similarities between the synthetic sequences obtained with this monodomain approach and the sequences observed along a real fault zone, it seems more reasonable to concentrate on the formation and the evolution of a population of faults (Narteau 2006).

4.3 Acceleration of the seismic energy release

From this model it is possible to recognize seismic precursory phenomena for large event when $A < 0.5$. Akin to other critical point approaches, acceleration of the seismic energy release before main events has been documented by Varnes (1989), Sykes & Jaume (1990), Bufe & Varnes (1993), Bowman *et al.* (1998), Main (1999) and Zöller *et al.* (2001). A recent review of the literature on the subject and of the known underlying mechanism can be found in Sammis and Sornette (2002). Although the acceleration of the seismic energy release has been observed at a regional scale and not only along a single fault zone, one can try to compare these observations with synthetic sequences of foreshocks obtained for $A < 5$. In particular, basic statistical parameters such as the slope of the Gutenberg–Richter relationship and the total amount of stress dissipation can be determined over different time period.

Nevertheless, the real-space renormalization group approach is powerful from a qualitative point of view but is known to involve uncontrolled approximations as the quantitative level. Furthermore, when $0.5 < A < 5$ major events occur in a more chaotic fashion without precursors. Therefore, they are hard to predict. This work confirms that system in a near-critical state are inherently more unpredictable: large fluctuations in correlation length can occur with small changes in system energy. In addition, spatial clustering of seismic events shows that earthquakes on neighbouring fault zones may trigger each other. This behaviour cannot be considered in the scope of this model of a single fault zone. Therefore, the detailed regional arrangement of faults need also to be taken into account to discuss the seismic patterns (Narteau 2006).

4.4 A phase diagram approach

Phase diagrams allow to describe the critical state of the system and the seismogenic potential of a fault over short and long time, through a set of trajectories that can be called *attractors*. It is possible to distinguish different regions of the phase diagram on the basis of the observed sequences of events along these trajectories (Fig. 7):

(i) The seismic noise zone is characterized by regular small events. This behaviour is permanent for extremely low value of A ($A < 10^{-4}$) and observed during interseismic loading when $A < 0.5$. In the bottom left portion of the phase diagram (Fig. 7), the seismic noise corresponds to microscopic fluctuations of both the stress and the state of fracturing.

(ii) The precursors zone is characterized by an acceleration of seismic energy release. At the end of the interseismic loading when $A < 0.5$, the excess of stress can only be eliminated when microfractures are produced. The organization of these microfractures at increasingly larger length scales enables the acceleration of the seismic energy release. In the upper left portion of the phase diagram (Fig. 7), it corresponds to the slowly decaying trajectories towards the critical point.

(iii) The main shock zone is characterized by large events. It follows the acceleration process when $A < 0.5$ and it includes all seismic patterns when $0.5 < A < 5$. In the middle of the phase diagram (Fig. 7), the main shock corresponds to the largest vertical jumps.

(iv) The creep zone is characterized by small events. It includes all the seismic patterns when $A > 10$ and intermittently follows swarms of earthquakes when $5 < A < 10$. In the upper right portion of the phase diagram (Fig. 7), the creep corresponds to small fluctuations of both the stress and the state of fracturing. Such behaviour cannot be observed for A-value lower than 5.

(v) The healing zone is characterized by an extremely low level of seismicity. It typically follows the aftershock sequences of major events when $A < 5$. In the bottom right portion of the phase diagram (Fig. 7), the healing is a transient state towards seismic noise.

Since an A-value is introduced to a given domain, it is theoretically possible to describe the present state of a fault zone from the past earthquake sequence. However, it is difficult to implement this approach along real fault zone because earthquakes catalogues are short and incomplete for a broad magnitude range. Moreover, stress perturbations resulting from fault interaction are likely to be essential for the timing of earthquakes.

4.5 Seismic patterns resulting from stress perturbations

In this section, stress perturbations are associated with discontinuous phenomena such as earthquakes. They are positive or negative and,

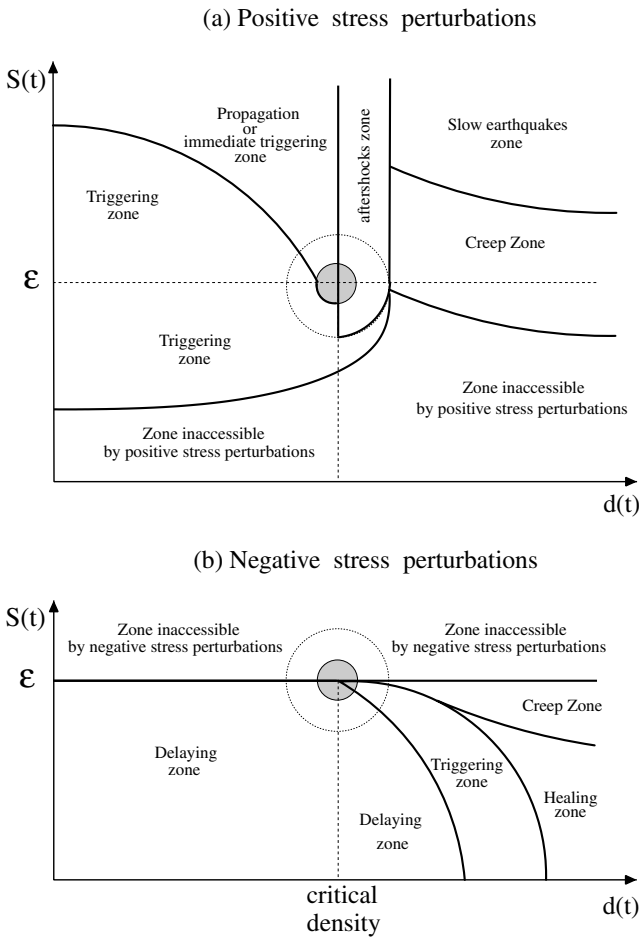

Figure 8. Schematic ($d(t)$, $s(t)$) phase diagrams following (a) positive and (b) negative stress perturbations along a fault segment. These phase diagrams indicate the impact of stress perturbations on the trajectories presented in Fig. 7. Each point corresponds to the density of microfractures $d(t)$ and the amount of shear stress stored in the system $s(t)$ just after stress perturbations. Then, the positions along the trajectories in Fig. 7 are obtained by vertical displacements. $\epsilon\sigma_s$ is the average shear stress stored in the system when largest events occur. Smaller concentric circles are associated with zones in which larger magnitude earthquakes occur (*critical point*).

in a phase diagram, they correspond to positive or negative vertical jumps. These displacements allow for more complex trajectories, for example, through zones unexplored by the trajectories which described the evolution of a fault segment (see Section 4.4 and Fig. 7).

In Fig. 8, the phase diagrams indicate how the fault segments has been perturbed under the assumption that stress perturbations do not occur in the future. For positive stress perturbations, it is possible to distinguish (Fig. 8a):

(i) *The triggering zone*: the behaviour of the fault segment is maintained but the next period of seismic activity will occur sooner.

(ii) *The propagation or immediate triggering zone*: the segment ruptures. This zone is only accessible through large stress perturbations or on segments which are close to their rupture thresholds.

(iii) *The aftershocks zone*: the segment has a high density of microfractures and only produces aftershocks.

(iv) *The slow earthquakes zone*: the segment eliminates its excess of stress by continuous slip. This zone is only accessible through large stress perturbations.

(v) *The creep zone*: the segment eliminates its excess of stress by continuous motions. The difference with the slow earthquakes zone is the amplitude of the stress reached after the stress perturbation. If the segment is already creeping only an acceleration may be observed (Murray & Segall 2005).

For negative stress perturbations, it is possible to distinguish (Fig. 8b):

(i) *The delaying zone*: the behaviour of the fault segment is maintained except that the next period of seismic activity will occur later.

(ii) *The healing zone*: creep stops for a limited time.

(iii) *the triggering zone*: the negative stress perturbation reduces the amplitude of the fracturing process. The relative higher amplitude of the healing process results in a lower density a microfractures. It favours the strengthening of some parts of the fault. Because the external loading is high, the strengthening may produce a significant seismic activity along the segment. The time interval between this activity and the stress perturbation is determined by the intensity of the stress perturbations and the intensity of the external loading.

Such an analysis of the stress perturbation along a single segment shows the wide variety of behaviours that can be expected if faults of different lengths interact. Future works will concentrate on this point, especially during the formation and the evolution of a population of faults (Narteau 2006).

5 CONCLUSION

A hierarchical model of rupture of a fault segment under constant loading reproduces different properties of the natural seismicity. Characteristic seismic sequences are presented with respect to the magnitude of a dimensionless parameter A, the ratio between the characteristic time of loading and the characteristic time of healing. If $A < 1$ the system is in a subcritical state controlled by faulting. From low to high A-value, the synthetic catalogues successively exhibit seismic noise, seismic swarms and major earthquakes with an acceleration of the seismic release or seismic precursors. If $A > 1$ the system is in a subcritical state controlled by healing. From high to low A-value, the synthetic catalogues successively exhibit seismicity associated with creep and diffuse seismic swarms. If $A \approx 1$ the system is in a critical state and, in addition to the seismic patterns described at different A-value, clusters of major earthquakes may be observed.

In the model, as the frequency of large events increases the total stress stored within the fault zone decreases. This observation is described as a weakening process.

A phase diagram offers an alternative to the seismic cycle picture. For different A-value, different trajectories indicate the seismic activity during consecutive stages of the seismic cycle. Via the phase diagram, an analysis of the stress perturbation shows a vast variety of phenomena associated with fault interactions.

ACKNOWLEDGMENTS

I would like to thank Russ Evans and three anonymous reviewers for helpful comments. I am grateful to J. Ritsema for his work on a previous version of this paper. The paper was improved by the constructive comments and thoughtful suggestions of I. Main. In the California Institute of Technology, Clément Narteau was supported through a Lavoisier fellowship from the French Ministry of Foreign Affairs. In the University of Edinburgh, Clément Narteau was supported through a Marie Curie fellowship No HPMFT-2000-00669

from the European Communauty. In I.P.G.P., Clément Narteau benefit from a Marie Curie reintegration grant 510640-EVOROCK of the European Community and from a Specific Targeted Research Project of the European Community (12975-E2C2).

REFERENCES

Allègre, C.J., Le Mouël, J.L. & Provost, A., 1982. Scaling rules in rock fracture and possible implications for earthquake prediction, *Nature,* **297,** 47–49.

Allègre, C.J., Le Mouël, J.L., Chau, H.D. & Narteau, C., 1995. Scaling organization of fracture tectonics (S.O.F.T.) and earthquake mechanism, *Phys. Earth planet. Int.,* **92,** 215–233.

Ben-Zion, Y., 2001. Dynamic ruptures in recent models of earthquake faults, *J. Mech. Phys. Solids,* **49,** 2209–2244.

Blanter, E.M. & Shnirman, M.G., 1997. Simple hierarchical system: stability, S.O.C and catastrophiques behavior, *Phys. Rev. E,* **55,** 6397–6403.

Bowman, D., Oullion, G., Sammis, C., Sornette, A. & Sornette, D., 1998. An observational test of the critical earthquake concept, *J. geophys. Res.,* **103,** 24 359–24 372.

Bufe, C. & Varnes, D., 1993. Predictive modeling of the seismic cycle of the greater San Francisco Bay region, *J. Geophys. Res.,* **98,** 9871–9883, 1993.

Gabrielov, A., Zaliapin, I., Newman, W.I. & Keilis-Borok, V.I., 2000. Colliding cascades model for earthquake prediction, *Geophys. J. Int.,* **143,** 427–437.

Kadanoff, L., 1966. The introduction of the idea that exponents could be derived from real-space scaling arguments, *Physics,* **2,** 263.

Kanamori, H. & Allen, C., 1986. Earthquake repeat time and average stress drop, in *Earthquake Source Mechanics,* pp. 227–235, AGU Geophys. Monogr.

Kolmogorov, A., 1941a. The local structure of turbulence in incompressible viscous fluid for very large Reynolds number, *Dokl. Akad. Nauk. SSSR,* **30,** 9–13.

Kolmogorov, A., 1941b. Dissipation of energy in locally isotropic turbulence, *Dokl. Akad. Nauk. SSSR,* **32,** 16–18.

Kraichnan, R., 1967. Inertiel ranges in two-dimensionnal turbulence, *Phys. Fluids,* **10,** 1417–1423.

Li, Y.-G., Vidale, J.E., Aki, K., Xu, F. & Burdette, T., 1998. Evidence of shallow fault zone strengthening after the 1992 M7.5 Landers, California, earthquake, *Nature,* **279,** 217–219.

Main, I., 1999. Applicability of time-to-failure analysis to accelerated strain before earthquakes and volcanic eruptions, *Geophys. J. Int.,* **139,** F1–F6.

Main, I.G., 1996. Statistical physics, seismogenic, and seismic hazard, *Rev. Geophys.,* **34,** 433–462.

Murray, J.R. & Segall, P., 2005. Spatiotemporal evolution of a transient slip event on the San Andreas fault near Parkfield, California, *J. geophys. Res.,* p. B09407.

Narteau, C., 2006. Formation and evolution of a population of strike-slip faults in a multiscale cellular automaton model, *Geophys. J. Int.,* doi:10.1111/j.1365-246X.2006.03213.x

Narteau, C., Allègre, C.J., Le Mouël, J.L. & Shebalin, P., 1997. Cascading up and down in the nucleation-growth process of S.O.F.T., *Eos, A.G.U. Fall Meeting, Abstracts,* **78,** 464.

Narteau, C., Shebalin, P., Holschneider, M., Le Mouël, J.L. & Allègre, C.J., 2000. Direct simulation of the stress redistribution in the scaling organization of fracture tectonics, *Geophys. J. Int.,* **141,** 115–135.

Narteau, C., Shebalin, P. & Holschneider, M., Temporal limits of the power law aftershock decay rate, *J. geophys. Res.,* **107,** doi:10.1029/2002JB001,868.

Narteau, C., Shebalin, P., Zöller, G., Hainzl, S. & Holschneider, M., 2003. Emergence of a band-limited power law in the aftershock decay rate of a slider-block model of seismicity, *Geophys. Res. Lett.,* **30,** doi:10.1029/2003GL017,110.

Narteau, C., Shebalin, P. & Holschneider, M., 2005. Onset of power law aftershock decay rates in Soutern California, *Geophys. Res. Lett.,* **32,** doi:10.1029/2005GL023,951.

Reynolds, P., Klein, W. & Stanley, H., 1977. Renormalization group for site and bond percolation, *Phys. C,* **10,** 167–172.

Reynolds, P., Stanley, H. & Klein, W., 1978. Percolation by position-space renormalisation group with large cells, *Phys. A,* **11,** 199–207.

Rotwain, I., Keilis-Borok, V. & Botvina, L., Premonitory transformation of steel fracturing and seismicity, *Phys. Earth planet. Int.,* **101,** 61–71.

Sammis, S. & Sornette, D., 2002. Positive feedback, memory and the predictability of earthquakes, *Proc. Nat. Acad. Sci. USA,* **99,** 2501–2508.

Scholz, C., Aviles, C. & Wesnousky, S., 1986. Scaling differences between large intraplate and interplate earthquakes, *Bull. seism. Soc. Am.,* **76,** 65–70.

Scholz, C.H., 1990. *The Mechanism of Earthquakes and Faulting,* Cambridge University Press, Cambridge, UK.

Schwartz, D. & Coppersmith, K., 1984. Fault behavior and caracteristic earthquake: examples from the Wasatch and San Andreas fault zones, *J. geophys. Res.,* **89,** 5681–5698.

Shimazaki, K. & Nakata, T., 1980. Time-predictable recurrence model for large earthquake, *Geophys. Res. Lett.,* **7,** 279–282.

Smith, W.D., 1986. Evidence for precursory changes in the frequency-magnitude *b*-value, *Geophys. J. R. astr. Soc.,* **86,** 815–838.

Sykes, L.R. & Jaume, S.C., 1990. Seismic activity on neighbouring faults as a long-term precursor to large earthquakes in the San Francisco Bay area, *Nature,* **348,** 595–599.

Trifu, C.-I. & Mircea, R., 1991. Frequency-magnitude distribution of earthquakes in Vrancea: relevance for a discrete model, *J. geophys. Res.,* **96,** 4301–4311.

Turcotte, D., Newman, W. & Gabrielov, A., 2000. A statistical physics approach of earthquakes, *Geophysical Monograph,* **120,** 83–96.

Turcotte, D.L., 1999. Seismicity and self-organized criticality, *Phys. Earth planet. Int.,* **111,** 275–293.

Varnes, D., 1989. Predicting earthquakes by analysing accelerating precursory seismic activity, *Pure appl. Geophys.,* **130,** 4407–4412.

Wilson, K.G., 1983. The renormalization group and critical phenomena, *Rev. Modern Physics,* **55,** 583–600.

Zöller, G., Hainzl, S. & Kurths, J., 2001. Observation of growing correlation length as an indicator for critical point behavior prior to large earthquakes, *J. geophys. Res.,* **106,** 2167–2175.